ACS APPLIED MATERIALS & INTERFACES

Research Article

Cite This: ACS Appl. Mater. Interfaces 2017, 9, 36137-36145

www.acsami.org

Highly Efficient and Air-Stable Infrared Photodetector Based on 2D Layered Graphene−Black Phosphorus Heterostructure

Yan Liu,[†] Bannur Nanjunda Shivananju,[†,§] Yusheng Wang,[†] Yupeng Zhang,[‡,§] Wenzhi Yu,[†] Si Xiao,[‖] Tian Sun,[†] Weiliang Ma,[†] Haoran Mu,[†] Shenghuang Lin,[†] Han Zhang,[‡] Yuerui Lu,[⊥] Cheng-Wei Qiu,[‡,#] Shaojuan Li,[*,†] and Qiaoliang Bao[*,†,§]

[†]Institute of Functional Nano and Soft Materials (FUNSOM), Jiangsu Key Laboratory for Carbon-Based Functional Materials and Devices, and Collaborative Innovation Center of Suzhou Nano Science and Technology, Soochow University, Suzhou 215123, P. R. China

[‡]SZU-NUS Collaborative Innovation Centre for Optoelectronic Science & Technology, and Key Laboratory of Optoelectronic Devices and Systems of Ministry of Education and Guangdong Province, School of Electronic Science and Technology, and College of Optoelectronics Engineering, Shenzhen University, Shenzhen 518060, China

[§]Department of Materials Science and Engineering, and ARC Centre of Excellence in Future Low-Energy Electronics Technologies (FLEET), Monash University, Clayton, Victoria 3800, Australia

[‖]Hunan Key Laboratory for Super-Microstructure and Ultrafast Process Institute of Super-Microstructure and Ultrafast Process in Advanced Materials, School of Physics and Electronics, Central South University, Changsha 410083, China

[⊥]Research School of Engineering, College of Engineering and Computer Science, Australian National University, Canberra, 2601, Australia

[#]Department of Electrical and Computer Engineering, National University of Singapore, 4 Engineering Drive 3, Singapore 117583, Singapore

Supporting Information

ABSTRACT: The presence of a direct band gap and high carrier mobility in few-layer black phosphorus (BP) offers opportunities for using this material for infrared (IR) light detection. However, the poor air stability of BP and its large contact resistance with metals pose significant challenges to the fabrication of highly efficient IR photodetectors with long lifetimes. In this work, we demonstrate a graphene−BP heterostructure photodetector with ultrahigh responsivity and long-term stability at IR wavelengths. In our device architecture, the top layer of graphene functions not only as an encapsulation layer but also as a highly efficient transport layer. Under illumination, photoexcited electron−hole pairs generated in BP are separated and injected into graphene, significantly reducing the Schottky barrier between BP and the metal electrodes and leading to efficient photocurrent extraction. The graphene−BP heterostructure phototransistor exhibits a long-term photoresponse at near-infrared wavelength (1550 nm) with an ultrahigh photoresponsivity (up to 3.3×10^3 A W^{-1}), a photoconductive gain (up to 1.13×10^9), and a rise time of about 4 ms. Considering the thickness-dependent band gap in BP, this material represents a powerful photodetection platform that is able to sustain high performance in the IR wavelength regime with potential applications in remote sensing, biological imaging, and environmental monitoring.

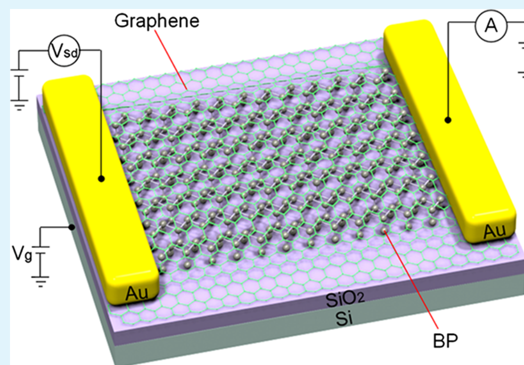

KEYWORDS: *IR photodetector, BP, graphene, heterostructure, responsivity, gain, stability*

1. INTRODUCTION

Graphene has been demonstrated to be an appealing alternative to traditional semiconductors because of its excellent optoelectronic properties and successful applications in diverse fields, especially in photodetection.[1,2] Graphene photodetectors can convert a broad spectrum of light (ultraviolet [UV] to terahertz) into electrical signals, and this range is unmatched by any photodetector based on traditional semiconductors. However, the low responsivity intrinsic to graphene photodetectors is a potential drawback because graphene lacks a band gap and has a low optical absorption (∼2.3%).[3] To overcome this shortcoming, various types of graphene-based photodetectors with different device configurations have been successfully demonstrated, such as coupling graphene with a

Received: July 7, 2017
Accepted: September 26, 2017
Published: September 26, 2017

© 2017 American Chemical Society

DOI: 10.1021/acsami.7b09889
ACS Appl. Mater. Interfaces 2017, 9, 36137−36145

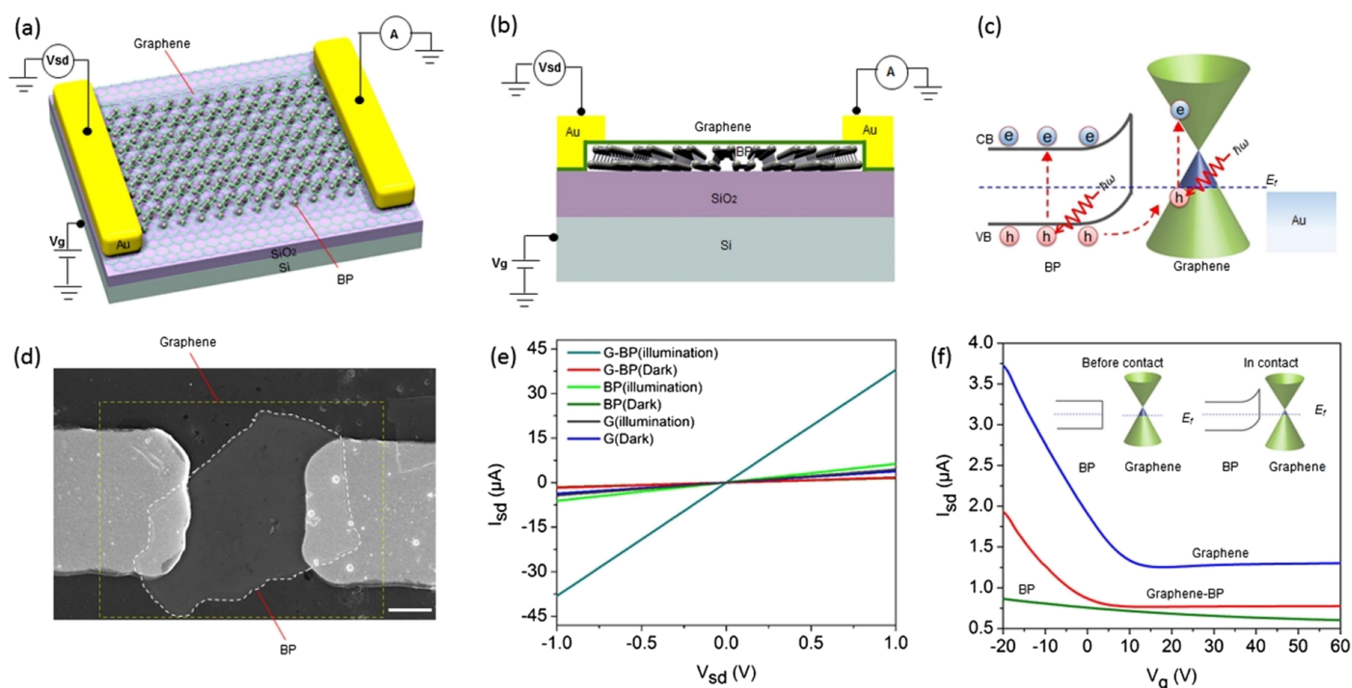

Figure 1. Graphene−BP heterostructure photodetector. (a) Three-dimensional schematic diagram of the graphene−BP heterostructure photodetector, in which monolayer graphene is coated on top of the BP flake to enhance the photocurrent response at 1550 nm and protect BP from the external environment. (V_{sd}: source−drain voltage, I_{sd}: source−drain current, and V_g: gate voltage). (b) Schematic of the graphene−BP heterostructure-based photodetector and the circuit used to perform the two-terminal electrical measurements. (c) Band diagram of the graphene−BP heterostructure and the photoexcited hot carrier transport process under illumination corresponding to zero gate voltage (V_g); the dotted line represents the Fermi levels (E_F). (d) SEM image of the graphene−BP heterostructure device (the thickness of BP is ∼35 nm); scale bar: 2 μm. (e) *I*−*V* curves of the graphene−BP heterostructure, pure graphene, and pure BP photodetectors in the dark and under light illumination of 1550 nm wavelength. V_g = 0 V. (f) Transfer characteristics of the graphene−BP heterostructure, pure BP, and pure graphene photodetectors determined in the dark at room temperature. V_{sd} = 0.5 V.

microcavity,[4] quantum dots,[5] and plasmonic nanostructures.[6] The most attractive and powerful strategy is to construct van der Waals heterostructures, in which graphene is integrated with another two-dimensional (2D) material that has a suitable band gap. To date, integrating graphene with layered transition metal dichalcogenides (TMDs), such as molybdenum disulfide[7] and tungsten diselenide,[8] which possess moderate band gaps and large optical absorptions (>10^7 m^{-1} across the visible range) compared with graphene, has been most extensively investigated. Graphene−TMD heterostructures have helped experimentally to verify the existence of strong light−matter interactions and ultrahigh photoresponsivities (greater than 10^7 A W^{-1}). However, photodetection is restricted to a narrow spectral bandwidth that mainly lies in the UV to visible wavelength range and is induced by TMDs' relatively large band gaps (1−2 eV).[9] Moreover, the responses of these devices are relatively slow because of the significantly smaller carrier mobilities (10 to ∼250 cm^2 V^{-1} s^{-1})[10,11] and relatively longer carrier relaxation times[12] of TMDs in comparison with those of graphene. These issues restrict their application for photodetection in near-infrared (NIR) wavelengths.[13] Combining graphene with a smaller band gap material (i.e., Bi_2Te_3, band gap: 0.3 eV) has been shown to be a feasible approach to expand the detection wavelength range from the visible to the NIR band.[14] However, significant improvements in the responsivity at NIR wavelengths especially at 1550 nm, which is limited by the low optical gain in Bi_2Te_3 for this particular wavelength range, are still needed.

Recently, a novel 2D material, black phosphorus (BP), has emerged as a candidate for electronic and optoelectronic applications.[15,16] BP is a 2D layered crystal with an orthorhombic crystal structure in which each phosphorus atom is covalently bonded to three neighboring phosphorus atoms within a plane.[17] This narrow band gap material has a layer-dependent direct band gap from 0.3 eV in the bulk to 1.8−2.0 eV for a monolayer,[16] which complements the photoresponse spectral ranges of semimetallic graphene and large band gap TMDs. In addition to its thickness-dependent band gap, BP also displays high carrier mobility on the order of 10 000 cm^2 V^{-1} s^{-1} in the bulk and 1000 cm^2 V^{-1} s^{-1} in flakes,[16] superior to those of TMDs, signifying that BP is a very promising 2D material for broadband and ultrafast optoelectronic applications,[18] particularly at IR wavelengths. However, one key challenge to using BP is its severe degradation,[19] which is caused by the layer-by-layer etching process during which it is exposed to oxygen and water molecules in the air.[20] Thereby, an encapsulation layer is needed to protect BP.[21,22] Furthermore, the large Schottky barriers between BP and metal electrodes significantly hinder the efficient transport of photocarriers, leading to a relatively low responsivity in most reported BP-based photodetectors.[18] Recently, a high-performance broadband BP-based short-channel photodetector in the wavelength range of 400−900 nm has been demonstrated with a record-high responsivity of 4.3 × 10^6 A W^{-1} at 633 nm.[23] Nevertheless, a highly efficient and air-stable IR photodetector, particularly at the technically important telecommunications band, based on BP has not been demonstrated. Here, we demonstrate a high-performance IR photodetector consisting of a graphene−BP vertical heterostructure with ultrahigh responsivity and long-term stability.

DOI: 10.1021/acsami.7b09889
ACS Appl. Mater. Interfaces 2017, 9, 36137−36145

2. EXPERIMENTAL SECTION

2.1. Preparation of the Graphene–BP Heterostructure. The graphene films were grown on a 25 μm copper foil (Alfa Aesar, United States) via chemical vapor deposition (CVD). A piece of glass is covered with a transparent plastic tape with a small hole in the center. Poly(methyl methacrylate) (PMMA)-coated graphene monolayer is transferred onto the plastic tape with a hole at the center. The glass substrate with a graphene monolayer is then attached to the three-axis micrometer stage. Separately, by using a blue sticky tape, BP flakes (smart-elements GmbH) with different thicknesses were transferred onto the SiO_2/Si substrate using the standard mechanical exfoliation method and placed under an optical microscope. Then immediately, the monolayer graphene is positioned upside down and transferred on top of the BP flake using a three-axis micrometer stage and an optical microscope. The PMMA polymer is later washed off with acetone.[24] Second, UV lithography and oxygen plasma etching techniques were utilized to selectively remove graphene, defining the area of the graphene–BP heterostructure.

2.2. Fabrication of the Photodetectors. The graphene–BP heterostructure was transferred on top of an oxidized Si substrate so that a gate voltage V_g could be applied. UV lithography was conducted to outline the device pattern, electron-beam evaporation was performed to deposit gold (Au) contacts with a thickness of 100 nm, and a lift-off technique was used to form the source and drain electrodes on top of graphene. For the electrical measurement, a direct current bias voltage (1 V) was applied to one Au contact (source), allowing the source–drain current (I_{sd}) to flow through the graphene–BP heterostructure and reach the other Au contact (drain).

2.3. Characterizations of the Graphene–BP Heterostructure. The surface morphologies of the graphene–BP heterostructure photodetectors were examined by a scanning electron microscopy (SEM) (Carl Zeiss, Supra 55) instrument. The thicknesses of the graphene–BP heterostructures were measured using an atomic force microscopy (AFM) (Bruker, Dimension Icon) instrument. The Raman spectra were collected using a micro-Raman system (Horiba Jobin Yvon, LabRAM HR 800) with a 514 nm excitation laser.

2.4. Photodetection Measurements. The optoelectronic measurements at 1550 nm were conducted using a Neaspec optical microscopy platform which is able to couple and focus a 1550 nm light beam onto a desired location of the graphene–BP photodetector, whereas the electrical properties of the devices were measured using a Keithley (2614B) double-channel source-meter. The device characteristics were measured at visible (635 nm laser) and NIR (980 nm laser) wavelengths using a probe station (Cascade M150) equipped with a semiconductor property analyzer (Keithley 4200). The broadband photocurrent was measured using a UV–visible–IR spectrometer (Newport, Pviv-211v) with a semiconductor property analyzer (Keithley 2612). All the measurements were performed at room temperature under ambient conditions.

2.5. Measurements of Carrier Dynamics. The carrier relaxation dynamics of the graphene–BP heterostructure was investigated by femtosecond optical pump–probe spectroscopy (Spectra-Physics, Spitfire ACE-35F-2KXP, Maitai SP and Empower 30) with the pump and probe lasers at 1550 nm and a pump power of 800 μW. Femtosecond pulses at 1550 nm were generated by a regenerative optical parametric amplifier (TOPAS, USF-UV2) seeded by a mode-locked oscillator.

3. RESULTS AND DISCUSSION

3.1. Graphene–BP Heterostructure Photodetector. Figure 1a shows the schematic diagram of a high-performance IR photodetector consisting of a graphene–BP vertical heterostructure. There are two important characteristics of this device configuration (Figure 1b). First, the encapsulation of monolayer graphene can effectively prevent unpredicted BP degradation, thus ensuring the long-term stability of the device under ambient conditions. Second, the direct contact between graphene and the source–drain electrodes provides a high-speed pathway for efficient charge carrier extraction because the energy barrier between graphene and Au is much smaller than that between BP and Au, as shown in Figure 1c. Under illumination, most of the photoexcited carriers (electron–hole pairs) are generated in the thick BP, in which the hole mobility is larger than the electron mobility.[16] The carriers are then separated and holes are injected into the top graphene layer, which is more conductive, leading to fast extraction of the photocurrent. Because of the perfect encapsulation by graphene, the enhanced light–matter interaction in the graphene–BP heterostructure, and the fast separation of the photocarriers between graphene and BP, these devices are expected to yield extraordinary photoresponses at IR wavelengths.

The formation of a graphene–BP heterostructure was achieved by sequentially transferring BP flakes and graphene onto the same location of a SiO_2 substrate. The standard mechanical exfoliation method was used to prepare BP flakes with different thicknesses (15–60 nm) from a bulk BP crystal. Then, a dry transfer technique was applied to cover the BP sample with a monolayer graphene film grown by CVD.[24] UV lithography was performed to outline the device pattern and the photoactive area in the channel, which was protected by graphene. Figure 1d shows a representative SEM image of the graphene–BP heterostructure device in which the BP flake is fully encapsulated by the monolayer graphene film. Raman spectroscopy was used to verify that BP is covered by the graphene film (Figure S1a). The morphology of the heterostructure was investigated using an AFM instrument (Figure S1b,c). Graphene was found to conform to the underlying BP very well without leaving any obvious bubbles or gaps through which air or other species could diffuse.

To investigate the photoresponse of the graphene–BP heterostructure, we compared the source–drain current (I_{sd}) of graphene–BP, pure BP, and pure graphene photodetectors at different source–drain voltages (V_{sd}), as shown in Figure 1e. Here, we present the results of a graphene–BP heterostructure in which BP is ~35 nm thick (Figure S1b). This BP flake corresponds to approximately 70 atomic layers, with a band gap of ~0.36 eV.[25–27] Figure 1e shows $I-V$ curves of the graphene–BP heterostructure, pure graphene, and pure BP photodetectors in the dark and under light illumination of 1550 nm wavelength. Also, the ratios for I_{photo}/I_{dark} of pure BP, pure graphene, and graphene–BP heterostructure photodetectors are 4.09, 1.15, and 22.05, respectively. The photocurrent derived from $I_{photo} - I_{dark}$ of Figure 1e is plotted in Figure S2a. Clearly, the graphene–BP heterostructure device exhibits a remarkable photocurrent approximately 60 times higher than that of the pure graphene device and 8 times higher than that of the pure BP device without the need for a gate bias. The large photocurrent mainly originates from the large photocarrier generation resulting from the strong light absorption in the multilayer BP and the efficient charge separation in the graphene–BP heterostructure. Large photoresponses were also observed when the devices were illuminated with visible light (635 nm, Figure S2b).

Figure 1f depicts the transfer characteristics of the devices operated in the dark at room temperature. It is worth noting that all three devices display a similar p-type polarity in their transfer curves. Graphene is known to be intrinsically semimetallic, and most carriers are holes because of the substrate doping effects caused by oxygen and molecular adsorption from the air.[28] The intrinsic doping level and Fermi

DOI: 10.1021/acsami.7b09889
ACS Appl. Mater. Interfaces 2017, 9, 36137–36145

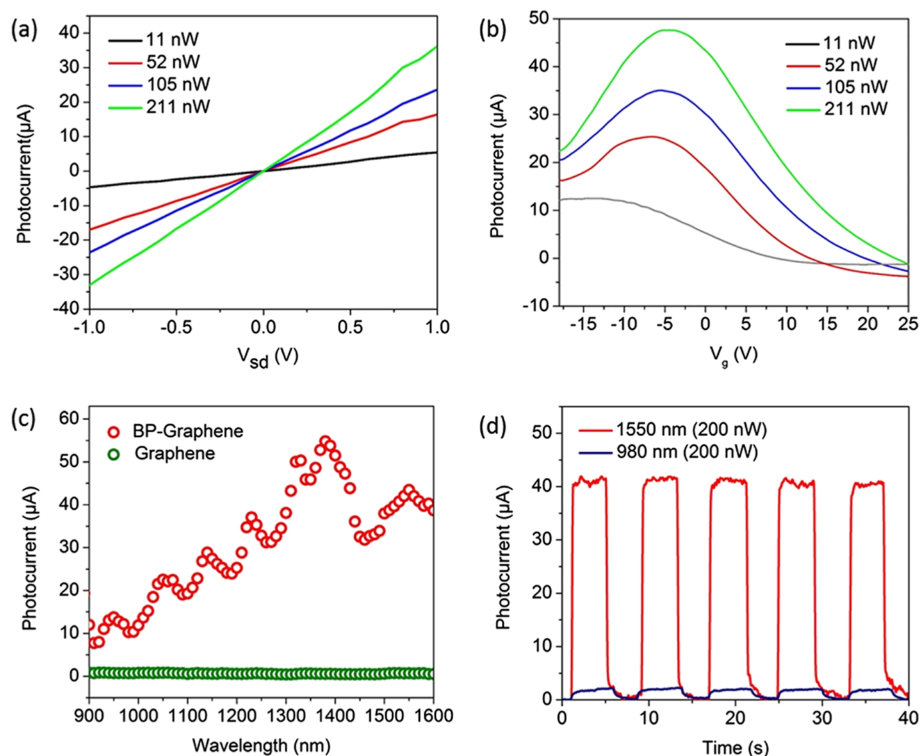

Figure 2. Broadband IR photoresponse of the graphene−BP heterostructure photodetector. (a) Magnitude of the photocurrent increases linearly with the source−drain bias voltage for different incident powers at 1550 nm and V_g = 0 V. (b) Photocurrent for different incident powers as a function of the gate voltage of the graphene−BP heterostructure detector with a source−drain bias (V_{sd}) of 1 V and an excitation wavelength (λ) of 1550 nm. (c) Dependence of the photocurrent on the excitation wavelength (from 900 to 1600 nm) for the graphene−BP and pure graphene devices with V_{sd} = 1 V. (d) Temporal photoresponses of the graphene−BP heterostructure photodetector at 1550 nm (200 nW) and 980 nm (200 nW) with V_{sd} = 1 V and V_g = 0 V.

energy of monolayer graphene can be determined by the transfer characteristics while scanning the back-gate voltage (V_g). Meanwhile, BP is also a hole-transport-dominated semiconductor, as can be inferred from its transfer curve. With monolayer graphene in contact with the BP flake, the conventional theory of ideal metal−semiconductor contacts can be applied. In the absence of a gate or bias voltage, the E_F of the monolayer graphene sheet is located near the top of the BP valence band. Because of the work function mismatch between multilayer BP and monolayer graphene, the holes will move from graphene to BP, resulting in band bending at the interface (Figure 1f, inset). At equilibrium, the surface potential at the interface can be expressed as $V_S = \frac{W_{BP} - W_G}{q}$, where q is the electric charge, W_{BP} represents the work function of the BP flakes (i.e., ∼4.49 eV),[29] and W_G represents the work function of monolayer graphene (i.e., ∼4.6 eV).[30] The direction of the built-in electric field is from BP to graphene, and the role of graphene is like a surface p-doping for BP in the heterostructure. Meanwhile, the transfer curve of the graphene−BP heterostructure device shifts to the left (Figure 1f), compared to that of the pure graphene device, indicating that the graphene−BP device is less hole-doped. To confirm this, the Hall measurements of the monolayer graphene and graphene−BP heterostructure were conducted. The results of Hall measurements to calculate the hole concentration in graphene and BP are shown in section S3 of the Supporting Information. The average values for the hole concentration were 3.01 × 10^{12} cm^{-2} for monolayer graphene and 1.2 × 10^{12} cm^{-2} for graphene with a BP flake embedded beneath it, in agreement with the conclusion drawn above.

Because BP is less conductive than graphene, the carrier transport should mainly occur in graphene. The field-effect mobility was calculated according to $\mu_{FE} = \frac{\partial I_{sd}}{\partial V_g}\frac{L}{WC_{ox}V_{sd}}$, where I_{sd} is the source−drain current, V_g is the back-gate voltage, V_{sd} is the source−drain voltage, C_{ox} is the gate capacitance, L is the channel length (∼10.8 μm), and W is the channel width (∼8 μm). For the graphene−BP heterostructure device, the mobility is 6813 cm^2 V^{-1} s^{-1}, much higher than the previously reported mobility in pure BP transistors (400−1000 cm^2 V^{-1} s^{-1}).[15,16,18] This significantly enhanced field-effect mobility can be attributed to the fact that the transport occurs predominately in the graphene layer (intrinsic mobility above 10 000 cm^2 V^{-1} s^{-1}) and the decreased sheet resistance (R_S) of the graphene−BP heterostructure compared with those of the pure BP flakes; this is also the major reason underlying the enhanced output current in the graphene−BP heterostructure (Figure 1f). Considering the smaller band gap of BP, the graphene−BP device can overcome the major shortcomings of the graphene−TMD photodetectors in terms of operating speed and responsive spectral range and has great potential for ultrafast photodetection at NIR wavelengths.

3.2. Broadband Infrared Photoresponse. We next investigated the optoelectronic properties of our device, as shown in Figure 2, in which all the measurements were conducted at room temperature under ambient conditions. Figure 2a presents the photocurrent as a function of the source−drain bias (V_{sd}) at zero gate voltage under illumination

DOI: 10.1021/acsami.7b09889
ACS Appl. Mater. Interfaces 2017, 9, 36137−36145

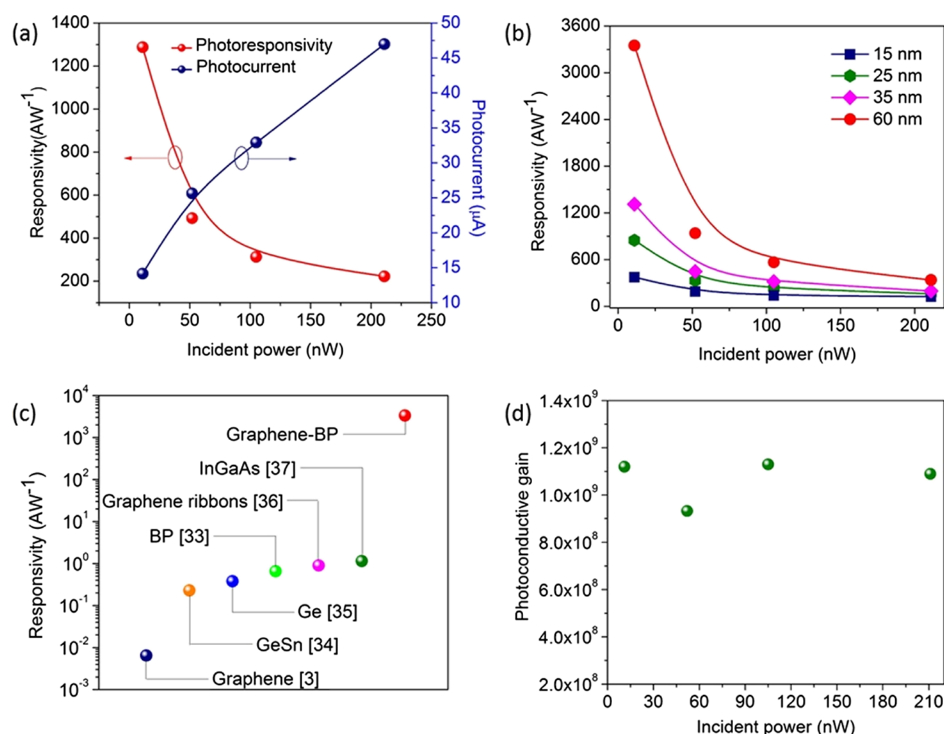

Figure 3. Figures-of-merit of the graphene−BP heterostructure at 1550 nm. (a) Photocurrent and photoresponsivity of the graphene−BP photodetector with respect to the incident power. (b) Responsivity of the graphene−BP heterostructures with different thicknesses as a function of the incident power. A high photoresponsivity of 3300 A W^{-1} at 60 nm is obtained for the thick BP flake covered with monolayer graphene. (c) Comparison of the photoresponsivity of the graphene−BP heterostructure photodetector with those of state-of-the-art photodetectors operating at 1550 nm. (d) Photoconductive gain of the graphene−BP photodetector as a function of the incident power.

from a 1550 nm laser with different laser powers. The black line shows the photocurrent for the low incident laser power (11 nW), which simply follows Ohm's law: $I = V_{sd}/R_s$, where R_s is the resistance of the graphene−BP heterostructure. The photocurrent increases linearly as V_{sd} varies from 0 to 1 or −1 V (Figure 2a) because of the increase in carrier drift velocity and the related reduction of the carrier transit time.[13] With increasing incident laser power (52, 105, and 211 nW), the photocurrent (I_{sd}) also increases because stronger light−matter interactions occur in the graphene−BP heterostructure, which results in the generation of more electron−hole pairs, leading to a net increase in the photocurrent. We note that for no bias voltage (V_{sd} = 0), the photocurrent is about zero, regardless of the power of the optical illumination. However, by applying a small source−drain bias, the photocurrent can be significantly enhanced.

To further elucidate the physical processes underlying the photocurrent generation in the graphene−BP heterostructure, the effect of illumination (λ = 1550 nm) on the transfer characteristics of the device at V_{sd} = 1 V was studied, as shown in Figure S4. Considering the fact that the photon energy (0.8 eV) is larger than the band gap in BP and the photogenerated carriers can be localized in BP, the photogating effect plays a dominant role to contribute to the photocurrent generation. We noted an obvious positive shift of the neutral point upon illumination because the increase in the majority carriers (i.e., holes) in the device is accompanied by a downshift of the E_F, indicating a photoinduced p-doping effect in graphene.

In particular, under illumination, the electron−hole pairs are generated in the BP flake, and the holes are transferred to graphene because of the built-in electric field between BP and graphene. Simultaneously, the electrons remain trapped in the BP film (Figure S4, inset). Consequently, the negative charges in the BP layer attract more holes in the graphene film, the so-called photogating effect,[5] and therefore, the transistor requires a higher gate voltage to reach the neutrality point.

The net photocurrent ($I_{light} - I_{dark}$) with varying gate voltages under different light powers is plotted in Figure 2b. The magnitude of the photocurrent is found to be gate-modulated, and the photocurrent increases with the light power. The maximum photocurrent occurs when the gate voltage is approximately −5 V, when the E_F is at the appropriate position for photoexcited holes to transfer from BP to graphene. We also noted that as the light intensity increases, the photocurrent peak slightly shifts to a higher gate voltage because the abundant trapped photogenerated electrons induce more holes in graphene, which needs more positive gate voltage to compensate. When sweeping V_g from negative to positive, the ambipolar switching of graphene is realized as the E_F shifts from the valence band into the conduction band. When applying a gate voltage of ∼20 V, the photocurrent falls to nearly zero because the injected electrons by gate completely recombine with the photoexcited holes. This tunable feature is highly important in photodetection because it offers a convenient way to control the device in terms of on−off switching.

The wavelength-dependent photocurrent of the graphene−BP heterostructure photodetector is shown in Figure 2c. Clearly, we can see that the graphene−BP device has a broadband photoresponse at NIR wavelengths from 900 to 1600 nm. The photocurrent varies nonlinearly with the wavelength and shows an ultrahigh photoresponse (∼45 μA) at 1550 nm for an incident power of 211 nW, which is 90 times higher than the value for pure graphene (∼0.5 μA) at this wavelength. Considering the fact that 70-layer BP is too thick

DOI: 10.1021/acsami.7b09889
ACS Appl. Mater. Interfaces 2017, 9, 36137−36145

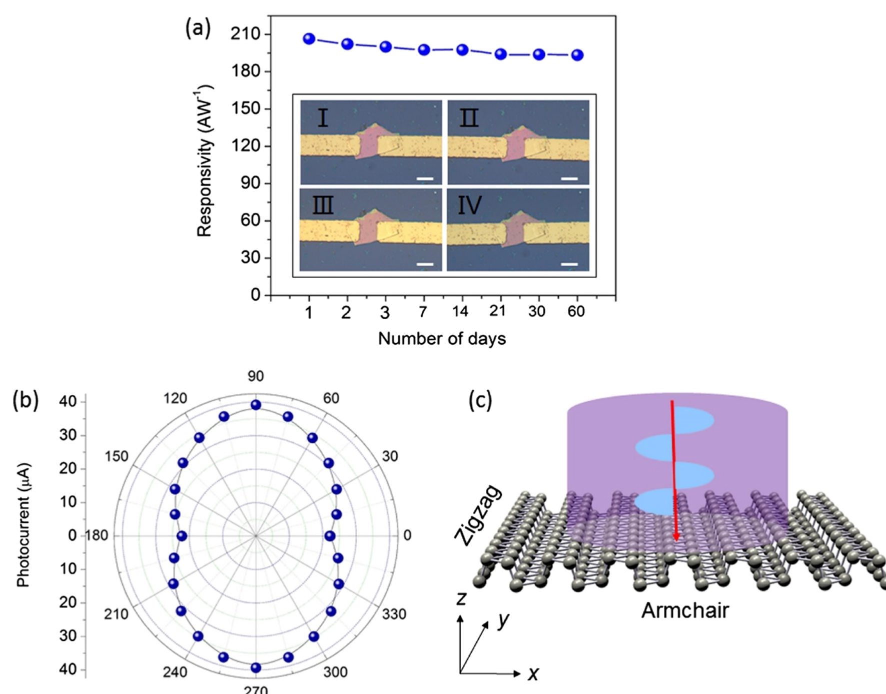

Figure 4. Stability and polarization-dependent photoresponse results of the graphene−BP heterostructure photodetector. (a) Responsivity of the graphene−BP photocurrent as a function of exposure time with a laser power of 211 nW; the thickness of the graphene−BP heterostructure is 35 nm. Inset: Optical images of the graphene−BP heterostructure photodetector as a function of time (I: 1 day, II: 7 days, III: 30 days, and IV: 60 days; all scale bars are 8 μm). The device characterization was performed in air at room temperature. (b) Photocurrent can be tuned by varying the polarization angle of the incident 1550 nm light. (c) Crystal structure of BP showing phosphorus linked along the *x*-axis, *y*-axis, and *z*-axis.

to show excitonic peaks,[25,31] the wavelength-dependent oscillation in photocurrent is likely due to the interference from the SiO_2/Si substrate. To further confirm this, we prepared BP photodetector devices on a polyethylene naphthalate substrate that does not have a thin dielectric capping layer and did not observe significant peaks in photocurrent (see Figure S5).

The temporal photoresponse of our device was investigated under ambient conditions, as shown in Figure 2d. The photocurrent can be effectively modulated when the light is turned on and off periodically in seconds with V_{sd} = 1 V. A stable photocurrent of approximately 40 μA can be observed in the "on" state for a wavelength of 1550 nm (200 nW), which is two times higher than that at 635 nm under 500 nW light power (Figure S6a). The response (rise) times of the graphene−BP heterostructure photodetector are at the scale of a few milliseconds (see Figure S7). The response is close to those of pure BP-based photodetectors with a similar device configuration[32] and slower than those of waveguide-integrated BP[33] photodetectors because of the limitation of the measurement electronics.

3.3. Figures-of-Merit at the Infrared Wavelength. To gain further insights into the capacity of the graphene−BP device for NIR photodetection, we plotted the power-dependent photoresponse and calculated the photoresponsivity at a fixed wavelength of 1550 nm, as depicted in Figure 3a. The magnitude of the photocurrent increases as the light power increases from 11 to 211 nW. Under the low illumination power of 11 nW, the device shows an ultrahigh responsivity of 1.3×10^3 A W^{-1} at 1550 nm, which is approximately 213 000 times higher than that of the pure monolayer graphene device[3] and nearly 2000 times higher than that of the recently reported pure BP phototransistor.[16,18]

Notably, the photoresponsivities of the graphene−BP device at other wavelengths, such as 635 and 980 nm, are also significantly higher than those of the pure BP device (Figures S6b and S8). To explore the performance limit of the graphene−BP heterostructure, we fabricated many devices with BP layers of different thicknesses. As the number of layers of BP increases, the energy spacing between two adjacent subbands within the conduction or valence bands decreases monotonically, which results in the enhancement of the IR wavelength absorption.[25] Moreover, a thicker BP layer has higher carrier mobility as compared to a thinner BP layer.[16] Thereby, thicker BP layers were found to deliver even higher photocurrents (Figure S9) and photoresponsivities (Figure 3b). For example, the graphene−BP heterostructure with 60 nm thick BP achieves the highest photoresponsivity of 3300 A W^{-1} at 1550 nm.

To further demonstrate the sensitivity of our device, we compared the photoresponsivity of our graphene−BP heterostructure detector with those found for previously reported photodetectors operating at 1550 nm,[3,33−37] as presented in Figure 3c. Our graphene−BP photodetector outperforms other photodetectors based on conventional semiconductor materials. In particular, the photoresponsivity is 3046 times better than the state-of-the-art InGaAs detector operating at 1550 nm,[37] indicating the great potential of the graphene−BP heterostructure for applications in biological imaging, remote sensing, environmental monitoring, and optical communication.

The photoconductive gain of the graphene−BP heterostructure at 1550 nm was calculated and is shown in Figure 3d. The detailed calculation of the photoconductive gain of the graphene−BP heterostructure photodetector is shown in section S10 of the Supporting Information. In the equation

DOI: 10.1021/acsami.7b09889
ACS Appl. Mater. Interfaces 2017, 9, 36137−36145

$G = \tau/t_L$,[5,38] τ represents the lifetime of the photoinduced carriers and t_L is the carrier transit time ($t_L = L^2/\mu V_{sd}$), where L is the channel length (L = 10.8 μm) of the device, V_{sd} is the source−drain voltage (V_{sd} = 1 V), and μ is the field-effect carrier mobility (μ = 6813 cm^2 V^{-1} s^{-1}). As described previously, because of the photogating effect, the lifetime of the photocarrier (τ) is increased,[5] which leads to a large photoconductive gain. Accordingly, we determined the highest photoconductive gain at 1550 nm under an incident power of 105 nW to be ∼1.13 × 10^9, which is 10^8 times higher than those of graphene[39] and BP[40] at this particular wavelength.

3.4. Long-Term Stability, Polarization-Dependent Photoresponse, and Pump−Probe Measurements. To confirm the long-term stability of our devices, device characterization as a function of aging time was performed under ambient conditions, as shown in Figure 4a. The photoresponsivity of the graphene−BP device degraded slightly from 206.44 to 193.33 A W^{-1} after 60 days under the same illumination conditions. The change in photoresponsivity was approximately 6%, suggesting that this device's stability under ambient conditions was greatly improved relative to that of its pure BP counterpart, which is very important for the practical implementation of this device in long-term operation.

Additionally, we investigated the polarization-dependent photoresponse of our devices, as shown in Figure 4b. Interestingly, the photocurrent of the graphene−BP heterostructure device also shows polarization dependence that varies with 180° rotational symmetry. Specifically, the maximum photocurrent of 39 μA is obtained when the polarization of the incident 1550 nm light is approximately 90° or 270°, corresponding to the x-axis of the crystal (Figure 4c). By contrast, the minimum photocurrent of 22 μA is observed at approximately 180° and 360°, when the incident light polarization is along the y-axis. This polarization dependence of the photocurrent is similar to that observed for pure BP-based photodetectors,[41] although the photocurrent is substantially larger. This phenomenon is mainly caused by the anisotropic band structure of BP, which leads to a direction-dependent interband optical transition.[26]

As indicated in previous studies, the interband transitions between the valence band maximum and the conduction band minimum for polarization along the x-axis (90° and 270°) are allowed, whereas those along the y-axis (0° and 180°) are partly forbidden.[42] Consequently, more polarized photons can be absorbed along the x-axis by a factor of 1.8 than along the y-axis, resulting in higher photocurrent along the x-direction. Thus, the graphene−BP heterostructure is suitable for the highly efficient detection of polarized IR light.

The carrier relaxation dynamics of graphene−BP heterostructure on the SiO_2/Si substrate is investigated by femtosecond optical pump−probe spectroscopy (1550 nm), as shown in Figure S11a. The density of the pump (1550 nm) light is about 0.84 GW/cm^2. The experimental results show that the graphene−BP heterostructure exhibits a fast optical relaxation within 41 fs after photoexcitation, a remarkable rate for van der Waals heterostructures. Compared with the carrier relaxation dynamics of pure graphene at 1550 nm (τ = 45 fs, see Figure S11b), the relaxation time of the graphene−BP heterostructure is slightly reduced (τ = 41 fs) because the direct band gap BP undergoes fast intraband relaxation (23 fs, see Figure S11c). The detail femtosecond optical pump−probe spectroscopy experiment (at 1550 nm) of the graphene−BP heterostructure is explained in section S11 of the Supporting Information. Such a short carrier relaxation time in van der Waals heterostructures can enable their applications for ultrafast optoelectronics at IR wavelengths.

4. CONCLUSIONS

In conclusion, we successfully demonstrated a highly efficient photodetector based on a graphene−BP heterostructure that operates at NIR wavelengths. Because the BP flakes exhibit large photon absorption over a broadband wavelength range, our graphene−BP heterostructure device exhibits not only broadband photodetection from the visible to IR wavelengths but also shows an ultrahigh photoresponsivity of ∼3.3 × 10^3 A W^{-1} at 1550 nm, which is 3046 times greater than those of previously reported photodetectors operating at the same wavelength. Regardless of the BP thickness, the devices exhibit qualitatively similar behaviors in terms of device performance; however, higher photoresponses were obtained using thicker BP flakes. In addition, the graphene−BP heterostructure photodetector shows a high photoconductive gain (1.13 × 10^9), an ultrafast charge transfer (41 fs), a polarization-dependent photocurrent response, and a long-term stability at 1550 nm. The high performance of this graphene−BP heterostructure photodetector paves the way for potential applications in remote sensing, biological imaging, and environmental monitoring using 2D materials.

■ ASSOCIATED CONTENT

Supporting Information

The Supporting Information is available free of charge on the ACS Publications website at DOI: 10.1021/acsami.7b09889.

Raman spectrum; AFM images; additional photoelectrical results at 1550, 635, and 980 nm; Hall measurements to calculate the hole concentration; wavelength-dependent photoresponse curve; thickness-dependent photoresponse curve; responsivity and gain calculation; and the details about pump−probe measurements (PDF)

■ AUTHOR INFORMATION

Corresponding Authors

*E-mail: sjli@suda.edu.cn (S.L.).
*E-mail: qiaoliang.bao@monash.edu (Q.B.).

ORCID

Yupeng Zhang: 0000-0003-2351-5579
Han Zhang: 0000-0002-2197-7270
Yuerui Lu: 0000-0001-6131-3906
Qiaoliang Bao: 0000-0002-6971-789X

Author Contributions

Y.L. and B.N.S. contributed equally. The manuscript was written through contributions from all authors. All authors have given approval to the final version of the manuscript.

Notes

The authors declare no competing financial interest.

■ ACKNOWLEDGMENTS

We acknowledge the support from the National Natural Science Foundation of China (nos. 61604102, 51222208, 51290273, and 91433107), the National Key Research & Development Program (no. 2016YFA0201902), the Youth 973 program (2015CB932700), ARC (DE120101569, DP140101501, and FT150100450), the China Postdoctoral Science Foundation (2014M550303 and 2014M551654), the

Doctoral Fund of Ministry of Education of China (grant no. 20123201120026), the Priority Academic Program Development of Jiangsu Higher Education Institutions (PAPD), and the Collaborative Innovation Center of Suzhou Nano Science and Technology. Q.B. acknowledges support from the Australian Research Council Centre of Excellence in Future Low-Energy Electronics Technologies (FLEET) (project number: CE170100039). C.-W.Q. acknowledges the financial support from A*STAR Pharos Programme (Grant No. 152 70 00014, with Project No. R-263-000-B91-305).

■ REFERENCES

(1) Bonaccorso, F.; Sun, Z.; Hasan, T.; Ferrari, A. C. Graphene Photonics and Optoelectronics. *Nat. Photonics* **2010**, *4*, 611−622.
(2) Bao, Q.; Loh, K. P. Graphene Photonics, Plasmonics, and Broadband Optoelectronic Devices. *ACS Nano* **2012**, *6*, 3677−3694.
(3) Mueller, T.; Xia, F.; Avouris, P. Graphene Photodetectors for High-Speed Optical Communications. *Nat. Photonics* **2010**, *4*, 297−301.
(4) Furchi, M.; Urich, A.; Pospischil, A.; Lilley, G.; Unterrainer, K.; Detz, H.; Klang, P.; Andrews, A. M.; Schrenk, W.; Strasser, G.; Mueller, T. Microcavity-Integrated Graphene Photodetector. *Nano Lett.* **2012**, *12*, 2773−2777.
(5) Konstantatos, G.; Badioli, M.; Gaudreau, L.; Osmond, J.; Bernechea, M.; de Arquer, F. P. G.; Gatti, F.; Koppens, F. H. L. Hybrid Graphene−Quantum Dot Phototransistors with Ultrahigh Gain. *Nat. Nanotechnol.* **2012**, *7*, 363−368.
(6) Echtermeyer, T. J.; Britnell, L.; Jasnos, P. K.; Lombardo, A.; Gorbachev, R. V.; Grigorenko, A. N.; Geim, A. K.; Ferrari, A. C.; Novoselov, K. S. Strong Plasmonic Enhancement of Photovoltage in Graphene. *Nat. Commun.* **2011**, *2*, 458.
(7) Roy, K.; Padmanabhan, M.; Goswami, S.; Sai, T. P.; Ramalingam, G.; Raghavan, S.; Ghosh, A. Graphene−MoS_2 Hybrid Structures for Multifunctional Photoresponsive Memory Devices. *Nat. Nanotechnol.* **2013**, *8*, 826−830.
(8) Kim, K.; Larentis, S.; Fallahazad, B.; Lee, K.; Xue, J.; Dillen, D. C.; Corbet, C. M.; Tutuc, E. Band Alignment in WSe_2−Graphene Heterostructures. *ACS Nano* **2015**, *9*, 4527−4532.
(9) Kumar, A.; Ahluwalia, P. K. Electronic Structure of Transition Metal Dichalcogenides Monolayers 1H-MX2 (M = Mo, W; X = S, Se, Te) from Ab-Initio Theory: New Direct Band Gap Semiconductors. *Eur. Phys. J. B* **2012**, *85*, 186.
(10) Fang, H.; Chuang, S.; Chang, T. C.; Takei, K.; Takahashi, T.; Javey, A. High-Performance Single Layered WSe_2P-FETs with Chemically Doped Contacts. *Nano Lett.* **2012**, *12*, 3788−3792.
(11) Fuhrer, M. S.; Hone, J. Measurement of Mobility in Dual-gated MoS_2 Transistors. *Nat. Nanotechnol.* **2013**, *8*, 146−147.
(12) Mai, C.; Semenov, Y. G.; Barrette, A.; Yu, Y.; Jin, Z.; Cao, L.; Kim, K. W.; Gundogdu, K. Exciton Valley Relaxation in a Single Layer of WS_2 Measured by Ultrafast Spectroscopy. *Phys. Rev. B: Condens. Matter Mater. Phys.* **2014**, *90*, 041414.
(13) Lopez-Sanchez, O.; Lembke, D.; Kayci, M.; Radenovic, A.; Kis, A. Ultrasensitive Photodetectors Based on Monolayer MoS_2. *Nat. Nanotechnol.* **2013**, *8*, 497−501.
(14) Qiao, H.; Yuan, J.; Xu, Z.; Chen, C.; Lin, S.; Wang, Y.; Song, J.; Liu, Y.; Khan, Q.; Hoh, H. Y.; Pan, C.-X.; Li, S.; Bao, Q. Broadband Photodetectors Based on Graphene−Bi_2Te_3 Heterostructure. *ACS Nano* **2015**, *9*, 1886−1894.
(15) Li, L.; Yu, Y.; Ye, G. J.; Ge, Q.; Ou, X.; Wu, H.; Feng, D.; Chen, X. H.; Zhang, Y. Black Phosphorus Field-Effect Transistors. *Nat. Nanotechnol.* **2014**, *9*, 372−377.
(16) Xia, F.; Wang, H.; Jia, Y. Rediscovering Black Phosphorus as an Anisotropic Layered Material for Optoelectronics and Electronics. *Nat. Commun.* **2014**, *5*, 4458.
(17) Brown, A.; Rundqvist, S. Refinement of the Crystal Structure of Black Phosphorus. *Acta Crystallogr.* **1965**, *19*, 684−685.
(18) Buscema, M.; Groenendijk, D. J.; Blanter, S. I.; Steele, G. A.; van der Zant, H. S. J.; Castellanos-Gomez, A. Fast and Broadband Photoresponse of Few-Layer Black Phosphorus Field-Effect Transistors. *Nano Lett.* **2014**, *14*, 3347−3352.
(19) Favron, A.; Gaufrès, E.; Fossard, F.; Phaneuf-L'Heureux, A.-L.; Tang, N. Y.-W.; Lévesque, P. L.; Loiseau, A.; Leonelli, R.; Francoeur, S.; Martel, R. Photooxidation and Quantum Confinement Effects in Exfoliated Black Phosphorus. *Nat. Mater.* **2015**, *14*, 826−832.
(20) Island, J. O.; Steele, G. A.; van der Zant, H. S.; Castellanos-Gomez, A. Environmental Instability of Few-Layer Black Phosphorus. *2D Mater.* **2015**, *2*, 011002.
(21) Avsar, A. Air-Stable Transport in Graphene-Contacted, Fully Encapsulated Ultrathin Black Phosphorus-Based Field-Effect Transistors. *ACS Nano* **2015**, *9*, 4138−4145.
(22) Doganov, R. A.; O'Farrell, E. C. T.; Koenig, S. P.; Yeo, Y.; Ziletti, A.; Carvalho, A.; Campbell, D. K.; Coker, D. F.; Watanabe, K.; Taniguchi, T.; Neto, A. H. C.; Özyilmaz, B. Transport Properties of Pristine Few-Layer Black Phosphorus by Van der Waals Passivation in an Inert Atmosphere. *Nat. Commun.* **2015**, *6*, 6647.
(23) Huang, M.; Wang, M.; Chen, C.; Ma, Z.; Li, X.; Han, J.; Wu, Y. Broadband Black-Phosphorus Photodetectors with High Responsivity. *Adv. Mater.* **2016**, *28*, 3481−3485.
(24) Castellanos-Gomez, A.; Buscema, M.; Molenaar, R.; Singh, V.; Janssen, L.; van der Zant, H. S. J.; Steele, G. A. Deterministic transfer of two-dimensional materials by all-dry viscoelastic stamping. *2D Mater.* **2014**, *1*, 011002.
(25) Zhang, G.; Huang, S.; Chaves, A.; Song, C.; Özçelik, V. O.; Low, T.; Yan, H. Infrared Fingerprints of Few-Layer Black Phosphorus. *Nat. Commun.* **2017**, *8*, 14071.
(26) Morita, A. Semiconducting Black Phosphorus. *Appl. Phys. A* **1986**, *39*, 227−242.
(27) Penumatcha, A. V.; Salazar, R. B.; Appenzeller, J. Analysing black phosphorus transistors using an analytic Schottky barrier MOSFET model. *Nat. Commun.* **2015**, *6*, 8948.
(28) Shi, Y.; Fang, W.; Zhang, K.; Zhang, W.; Li, L.-J. Photoelectrical Response in Single-Layer Graphene Transistors. *Small* **2009**, *5*, 2005−2011.
(29) Cai, Y.; Zhang, G.; Zhang, Y.-W. Layer-Dependent Band Alignment and Work Function of Few-Layer Phosphorene. *Sci. Rep.* **2014**, *4*, 6677.
(30) Shi, Y.; Kim, K. K.; Reina, A.; Hofmann, M.; Li, L.-J.; Kong, J. Work Function Engineering of Graphene Electrode via Chemical Doping. *ACS Nano* **2010**, *4*, 2689−2694.
(31) Low, T.; Rodin, A. S.; Carvalho, A.; Jiang, Y.; Wang, H.; Xia, F.; Neto, A. H. C. Tunable Optical Properties of Multilayer Black Phosphorus Thin Films. *Phys. Rev. B: Condens. Matter Mater. Phys.* **2014**, *90*, 075434.
(32) Buscema, M.; Island, J. O.; Groenendijk, D. J.; Blanter, S. I.; Steele, G. A.; van der Zant, H. S. J.; Castellanos-Gomez, A. Photocurrent Generation with Two-Dimensional Van Der Waals Semiconductors. *Chem. Soc. Rev.* **2015**, *44*, 3691−3718.
(33) Youngblood, N.; Chen, C.; Koester, S. J.; Li, M. Waveguide-Integrated Black Phosphorus Photodetector with High Responsivity and Low Dark Current. *Nat. Photonics* **2015**, *9*, 247−252.
(34) Su, S.; Cheng, B.; Xue, C.; Wang, W.; Cao, Q.; Xue, H.; Hu, W.; Zhang, G.; Zuo, Y.; Wang, Q. GeSn P-i-n Photodetector for All Telecommunication Bands Detection. *Opt. Express* **2011**, *19*, 6400−6405.
(35) Liu, J.; Cannon, D. D.; Wada, K.; Ishikawa, Y.; Jongthammanurak, S.; Danielson, D. T.; Michel, J.; Kimerling, L. C. Tensile Strained Ge P-i-n Photodetectors on Si Platform for C and L Band Telecommunications. *Appl. Phys. Lett.* **2005**, *87*, 011110.
(36) Chitara, B.; Panchakarla, L. S.; Krupanidhi, S. B.; Rao, C. N. R. Infrared Photodetectors Based on Reduced Graphene Oxide and Graphene Nanoribbons. *Adv. Mater.* **2011**, *23*, 5419−5424.
(37) Werner, L.; Friedrich, R.; Johannsen, U.; Steiger, A. Precise Scale of Spectral Responsivity for InGaAs Detectors Based on a Cryogenic Radiometer and Several Laser Sources. *Metrologia* **2000**, *37*, 523−526.
(38) Zhang, W.; Chuu, C.-P.; Huang, J.-K.; Chen, C.-H.; Tsai, M.-L.; Chang, Y.-H.; Liang, C.-T.; Chen, Y.-Z.; Chueh, Y.-L.; He, J.-H.; Chou,

M.-Y.; Li, L.-J. Ultrahigh-Gain Photodetectors Based on Atomically Thin Graphene-MoS_2 Heterostructures. *Sci. Rep.* **2014**, *4*, 3826.
(39) Zhang, B. Y.; Liu, T.; Meng, B.; Li, X.; Liang, G.; Hu, X.; Wang, Q. J. Broadband High Photoresponse from Pure Monolayer Graphene Photodetector. *Nat. Commun.* **2013**, *4*, 1811.
(40) Engel, M.; Steiner, M.; Avouris, P. Black Phosphorus Photodetector for Multispectral, High-Resolution Imaging. *Nano Lett.* **2014**, *14*, 6414−6417.
(41) Hong, T.; Chamlagain, B.; Lin, W.; Chuang, H.-J.; Pan, M.; Zhou, Z.; Xu, Y.-Q. Polarized Photocurrent Response in Black Phosphorus Field-Effect Transistors. *Nanoscale* **2014**, *6*, 8978−8983.
(42) Takao, Y.; Asahina, H.; Morita, A. Electronic Structure of Black Phosphorus in Tight Binding Approach. *J. Phys. Soc. Jpn.* **1981**, *50*, 3362−3369.

DOI: 10.1021/acsami.7b09889
ACS Appl. Mater. Interfaces 2017, 9, 36137−36145